IIETA International Information and Engineering Technology Association
Advancing the World of Information and Engineering

Revue des Composites et des Matériaux Avancés-Journal of Composite and Advanced Materials
Vol. 35, No. 6, December, 2025, pp. 1153-1161
Journal homepage: http://iieta.org/journals/rcma

Experimental Analysis of the Mechanical and Thermal Behaviour of Epoxy and Polyester GFRP Composites for Wind Turbine Blade Skin

Ferriawan Yudhanto[1*], Cahyo Budiyantoro[2], Mochamad Arif Irfa'i[3], Afri Arief Wicaksono[1], Ari Febriansyah[1]

[1] Department of Automotive Engineering Technology, Faculty of Engineering, Universitas Muhammadiyah Yogyakarta, Yogyakarta 55183, Indonesia
[2] Department of Mechanical Engineering, Faculty of Engineering, Universitas Muhammadiyah Yogyakarta, Yogyakarta 55183, Indonesia
[3] Department of Mechanical Engineering, Faculty of Engineering, Universitas Negeri Surabaya, Surabaya, Jawa Timur 60231, Indonesia

Corresponding Author Email: ferriawan@umy.ac.id

https://doi.org/10.18280/rcma.350615

Received: 30 October 2025
Revised: 27 November 2025
Accepted: 9 December 2025
Available online: 31 December 2025

Keywords:
wind turbine blade, polyester resin, epoxy resin, mechanical performance, thermal stability

ABSTRACT

This study evaluates the mechanical performance and thermal stability of glass fiber reinforced polymer (GFRP) with polyester and epoxy resin as polymer matrix for flexible skin applications in wind turbine blades. The composites were fabricated using the Vacuum Assisted Resin Transfer Moulding (VARTM) technique and tested through twist-tensile (ASTM D638) at angles of 0°, 20°, 40°, and 60°. Three-point bending tests (ASTM D790) were performed using 60 mm and 96 mm span configurations. The tensile test results revealed that GFRP-epoxy achieved a maximum strength of 334 MPa (0°), surpassing that GFRP-polyester, which exhibited reduced performance due to less optimal interfacial bonding. In the bending tests, GFRP-epoxy demonstrated superior performance with a strength of 519 MPa, while GFRP-polyester showed a significant reduction, particularly in the short span bending. Failure modes analysis using SEM revealed that GFRP-epoxy attained good fiber wetting and strong interfacial bonding. The GFRP-polyester composites were dominated by fiber pull-out, delamination, and debonding. The thermal stability of both is in the range 300℃ to 340℃. These findings confirm that GFRP-epoxy composite is more suitable as the primary matrix for a Horizontal Axis Wind Turbine (HAWT) blade due to its superior structural and thermal stability. In contrast, GFRP-polyester laminated composite is more appropriate for non-structural components with lower load demands.

1. INTRODUCTION

The transition to renewable energy has become a global priority to mitigate climate change. Indonesia targets Net Zero Emission (NZE) by 2060 and plans to expand wind power capacity to 597 MW by 2030 [1]. However, its current utilisation is still far below the target, reaching only 154.3 MW in 2024. One of the main challenges is the high cost of repairing wind turbine blades due to cracks in the transition zone on the blade, which significantly affects financial losses [2, 3]. According to Cavalcanti et al. [4], who conducted research in polymers, the results found that selecting matrix polymers has a fundamental role in determining wind turbine blades' structural, thermal, and economic performance.

The reliability of wind turbine blades plays a critical role in reducing maintenance expenses, as the transition zone of wind turbine blades are the most vulnerable component due to complex mechanical and environmental loads [5]. Validation is generally performed through full-scale testing under IEC 61400-23 standards to ensure structural safety, focusing on statistical loads and fatigue in flap-wise and edge-directions of blade wind turbine [6, 7]. While essential, these full-scale tests are costly and often insufficient to capture local failure mechanisms in blade subcomponents [8, 9]. Recent studies have emphasized the importance of subcomponent-level investigations, which can provide detailed insights into progressive damage phenomena such as delamination, debonding, and fiber fracture in composite turbine blades [10].

During operation, blades are subjected to a combination of tensile, torsional, and flexural loads, leading to critical shear stress between the skin and the core in sandwich composite structures [11]. Glass fiber reinforced polymer (GFRP) is commonly utilized as the primary skin material due to its favorable mechanical properties, including high specific strength, corrosion resistance, and relatively low cost [12, 13]. Recent works also highlight that GFRP offers stable performance under cyclic loading, making it a reliable choice for offshore and onshore wind turbine applications [14, 15].

Chen et al. [16] investigated the failure phenomena of the skin-core sandwich composite HAWT blade by combining static testing and FEA simulation on a large composite blade and using 3D failure criteria, showing an approach to understand skin and core cracks, including debonding and delamination. The Braga and Magalhaes [17] explained that glass fiber reinforced polymer matrix (GFRP) has good stability because the glass fiber inhibits polymer degradation as a matrix. Polymer resistance generally begins at the initial degradation temperature at 300℃.

Chichane et al. [18], have confirms that the prediction of composite mechanical properties is strongly influenced by fiber distribution, volume fraction, and matrix-reinforcement interactions. This study demonstrates that micromechanical models, such as the Halpin–Tsai models, effectively explain variations in modulus due to changes in composition and bond quality between components. These findings are relevant to the development of GFRP for wind turbine blade skins, where structural performance is determined mainly by the selection of the matrix and the stress transfer efficiency of the glass fibers. Halpin-Tsai prediction models integrated experimental and micromechanical approaches for epoxy and polyester composites to enhance the mechanical durability of wind turbine blades.

The manufacture of laminated composites with Vacuum Assisted Resin Transfer Moulding (VARTM) is a composite fabrication technique that utilises vacuum pressure to flow liquid resin into a stack of dry fibers hermetically sealed by bagging film. Once the vacuum is achieved, the resin is drawn through an inlet until all the fibers are evenly wetted. This process enhances impregnation, minimises voids, and yields a more controlled fiber volume fraction compared to conventional methods. VARTM is known for its efficiency in producing large structures and is capable of creating laminates with superior mechanical properties and consistency [19].

The novelty of this research is its focus on a comprehensive evaluation of the mechanical and thermal properties of wind turbine blade skin materials using twist-tensile and three-point bending test approaches. Unlike previous studies that focused on full-scale tests and numerical modelling, this study makes a new contribution by providing a local characterisation of HAWT blade skin materials through the integration of multi-angle twist-tensile tests (0°, 20°, 40°, 60°) and span-dependent flexural analysis. This study presents new design guidelines for the influence of fibers misalignment and span length on load transfer efficiency and resin selection in the blade transition zone, which is often damaged. No previous studies have analysed the mechanical behaviour of epoxy and polyester under combined twist–tension conditions that resemble blade transition loads.

2. MATERIALS AND METHOD

The graphical flowchart experimental process include Fabrication, testing, and characterization in this research shows on Figure 1.

2.1 Tensile test of GFRP composite

The materials comprised chopped strand mat (CSM) and woven roving (WR) 300gsm, comprising four layers (n_WR = 2 and n_CSM = 2) with a WR/CSM/WR/CSM stacking sequence. The GFRP composite was manufactured using a vacuum assisted resin transfer molding (VARTM) with 0.8 bar pressure. The tests were conducted to assess the material's response to twist-tensile and flexural loads, which are relevant to the working conditions of wind turbine blades. This experimental research focuses on the quality of the fiber-matrix bond reflected in changes in strength, stiffness, fracture strain, and failure modes. Two polymer materials were utilized: Yukalac BQTN 157-EX Polyester and GE 7118 Epoxy resin. Both polymers, curing time 24 hours and post cure 60° for two hours.

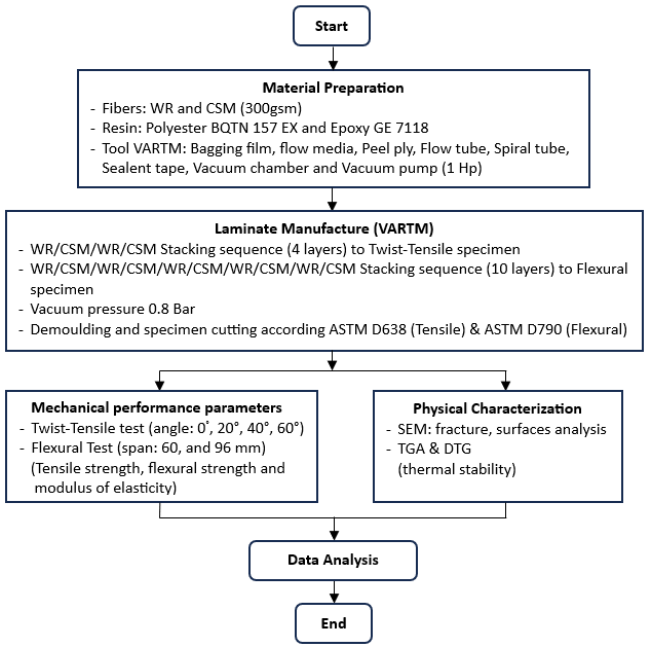

Figure 1. Research flowchart

Table 1. Properties of Yukalac BQTN 157 EX unsaturated polyester resin [20]

Number	Physical and Mechanical Properties	Value	Unit
1	Density	1.20	g/cm^3
2	Viscosity	4000-4500	mPa·s
3	Hardness	40	Barcol/G YZJ 934-1
4	Water absorption (25℃)	0.188	%
5	Flexural strength	92.1	MPa
6	Flexural Modulus	2.94	GPa
7	Tensile Modulus	3.0	GPa
8	Tensile Strength	55	MPa
9	Curing time	30-40	Minutes

Table 2. Properties of GE 7118 epoxy resin [21, 22]

Number	Physical and Mechanical Properties	Value	Unit
1	Density	1.18	g/cm^3
2	Viscosity	1400-1800	mPa·s
3	Hardness	85	Shore D
4	Water absorption (25℃)	0.15	%
5	Flexural Strength	105	MPa
6	Flexural Modulus	2.91	GPa
7	Tensile Strength	69	MPa
8	Tensile Modulus	3.03	GPa
9	Curing Time	120-150	Minutes

Tables 1 and 2 demonstrate that the two polymer matrices applied in this study have different physical and mechanical properties. Unsaturated Polyester Resin BQTN 157 EX was processed using methyl ethyl ketone peroxide (MEKPO) as an initiator with a resin to catalyst ratio of 100:1 (wt.%). Meanwhile, GE 7118 epoxy resin was combined with a hardener as a hardening agent with a *resin-to-hardener* ratio of 10:3 (wt.%). The difference in hardening mechanisms between the polyester and epoxy will affect the cross-linking density and, consequently, the mechanical performance of GFRP composites. The twist-tensile test specimen comprised four layers (n_WR = 2 and n_CSM = 2), with a fiber volume fraction (V_f) of 43% and a thickness of 1.1 mm. Figure 2(a) depicts the custom specimen with the upper and lower clamps mounted coaxially to the axis of the specimen, while the angle indicator is fixed to the clamp frame (Figure 2(b)).

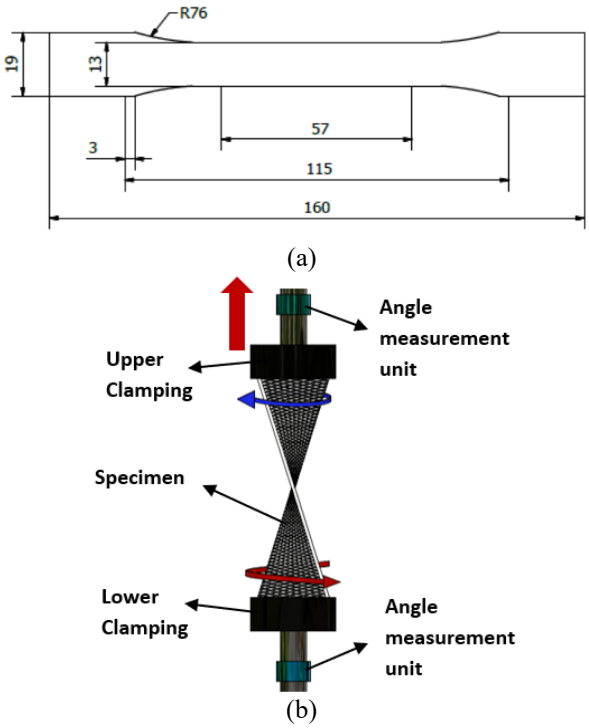

Figure 2. The GFRP composite specimen according (a) custom based ASTM D638 [23], and (b) custom JIG

2.2 Flexural test of GFRP composite

Flexural tests are essential because wind turbine blades are predominantly subjected to bending loads during operation due to continuous wind forces acting along their surfaces. These bending loads induce tensile stress on the bottom side and compressive stress on the top side. The flexural properties were evaluated using a three-point flexural method in accordance with ASTM D790, employing a Universal Testing Machine (UTM) with a load capacity of 25 kN and a crosshead speed of 5 mm/min.

Figure 3 shows that the flexural test was conducted using span lengths of 60 and 96 mm. The flexural specimen comprised ten layers (n_WR = 5 and n_CSM = 5), with a fiber volume fraction (V_f) of 46% and a thickness of 2.6 mm. The WR/CSM/WR/CSM/WR/CSM/WR/CSM/WR/CSM stacking sequence of GFRP composite specimens were cut to 13 mm width, 100 mm, and 150 mm overall length [24]. The minimum specimen employed was five to produce more uniform results and reduce deviations.

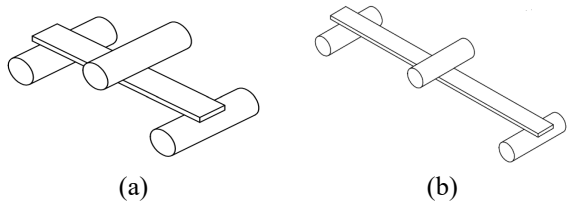

Figure 3. Scheme of flexural GFRP composite specimens, (a) span 60 mm and (b) span 96 mm

2.3 SEM image of failure mode

Scanning Electron Microscopy (SEM) analysis was performed on the fracture surfaces of tensile and flexural test specimens to identify the failure mechanisms of GFRP composites. The device deployed JEOL JSM-IT 210. SEM testing began with a sample preparation, where it was placed in the specimen holder to ensure a stable position and good electrical contact. The coating was carried out to coat the sample surface with platinum metal for 180 seconds using the sputter coating method, thereby providing a thin and even conductive layer without disturbing the surface morphology. After that, the sample was inserted into the SEM chamber and subjected to high vacuum conditions. Observations were conducted by adjusting test parameters, such as acceleration voltage, working distance, and magnification.

2.4 Thermal Gravimetric Analysis test

A Thermogravimetric Analysis (TGA) test was conducted using a NETZSCH STA 449 F3 Jupiter to determine the thermal stability and degradation characteristics of GFRP composite materials. The test was conducted in an inert nitrogen atmosphere with a 50 mL/min. gas flow rate to prevent oxidation. Composite specimens with a mass of approximately 5-10 mg were placed in an alumina crucible and heated from 26 to 600°C with a constant heating rate of 10°C/min. During heating, changes in mass were recorded against temperature to obtain the values of the onset temperature of degradation (T_{onset}), the maximum temperature of degradation (T_{max}), and the final residue that describes the glass fiber content in the composite.

3. RESULTS AND DISCUSSION

3.1 The Halpin-Tsai model

The Halpin-Tsai approach is a micromechanical model widely used to predict the modulus of elasticity fiber-reinforced composites. Unlike the Rule of Mixtures, which tends to provide an upper-bound estimate, the Halpin–Tsai model incorporates the effects of fiber geometry, orientation, fibers-to-matrix ratio, and stiffness, resulting in more realistic predictions for various types of composites, including short fibers and random orientations such as in CSM. The Table 3 is data sheet the E-glass fiber and polymer resin. The calculate fiber volume fraction and modulus of elasticity composite shows on Eqs. (1)-(3).

In general, the composite modulus is expressed in the equation:

$$E_c = E_m \frac{1+\eta V_f}{1-\eta V_f} \quad (1)$$

$$\eta = E_m \frac{(E_f / E_m)-1}{(E_f / E_m)+\xi} \quad (2)$$

$$V_f = \frac{mass\ per\ area}{\rho_f . t} \quad (3)$$

Note:

$E_c = Modulus\ of\ composite\ (GPa)$

$E_f = Modulus\ of\ fiber\ (GPa)$

$E_m = Modulus\ of\ matrix$ (GPa)

$V_f =$ Fiber volume fraction (%)

$\rho_f =$ Fiber density (gr/cm^3)

$\eta = reinforcement\ factor\ depend\ on\ geometry$

$\xi = shape\ orientation\ parameter$

$t = thickness\ (mm)$

$L = Length\ of\ fiber\ (mm)$

$d = diameter\ of\ fiber\ (mm)$

Note:

$\xi = 2\ for\ longitudinally\ oriented\ fibers$

$\xi = \frac{2.L}{d}\ for\ randomly\ oriented\ fibers$

Table 3. Properties data of polymer and E glass fiber

E_f (glass fiber) (GPa)	ρ_f (glass fiber) (g/cm^3)	Aspect Ratio (L/d) (mm)	E_m Polyester (GPa)	E_m Epoxy (GPa)
70	2.5	50/0.015	3.0 (tensile) 2.94 (Flexural)	3.03 (Tensile) 2.91 (Flexural)

From the Table 3, the tensile test specimen has a density is 2.5 g/cm^3. The four plies laminate (one ply WR or CSM is 300gsm), then to calculate the Fiber volume fraction (V_f):

$$V_f = \frac{4\ (plies).300\ g/cm^2}{2.5\ g/cm^3.0.11\ cm} = 43\%$$

Figure 4 shows that at a fiber volume fraction of 43%, the aligned fibers with a longitudinally oriented fiber factor $\xi = 2$ predict a modulus of composite (E_c) of approximately 6.7 GPa. In comparison, randomly oriented fibers (CSM), using $\xi = 2.L/d$, produce a predicted modulus of composite (E_c) of approximately 3 GPa.

3.2 Twist-tension analysis

Twist-tensile testing was performed to provide a more realistic description of the bond quality between resin and glass fibers under complex loading conditions. In conventional tensile testing, the dominant load was axial; thereby, not fully representing real conditions encountered in wind turbine blades, where the material experiences a combination of tensile and torsional loads. The test approach approximating real conditions is depicted on the angle measurement unit connected to a clamp or jig (Figure 5).

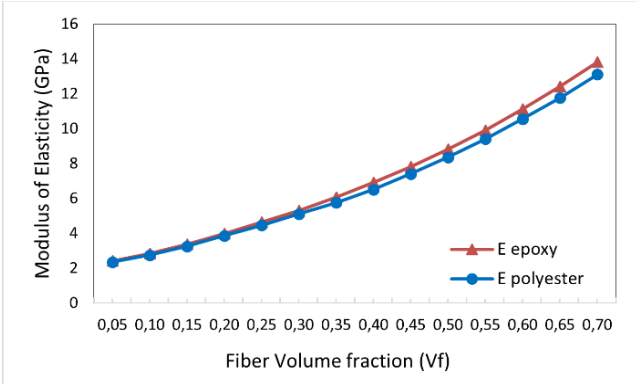

Figure 4. Prediction modulus of elasticity composite based on the Halpin-Tsai model

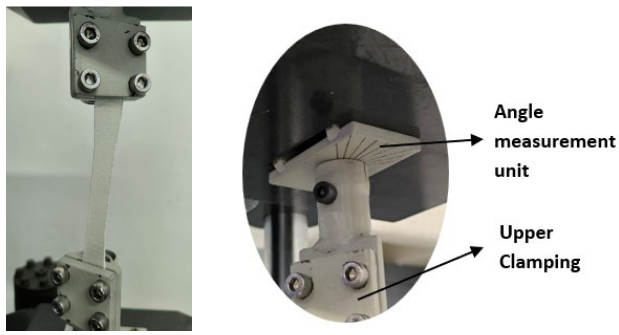

Figure 5. Twist-tensile of GFRP composite set on upper and bottom clamping with angle measurement

Figure 6(a) portrays that GFRP-epoxy resin exhibits significantly higher tensile strength (334 MPa) than GFRP-polyester (250 MPa) at 0° twist, indicating superior load transfer capability along the fiber direction. As the twist angle rose, GFRP-epoxy strength declined rapidly, particularly between 20° and 40°. At the same time, polyester remained relatively stable with a slight increase, suggesting better load distribution through fiber-matrix interaction at moderate angles. The at 60°, both resins experienced a significant drop, GFRP-epoxy (198 MPa) slightly lower than GFRP-polyester (203 MPa), signifying reduced stress transfer efficiency at high fiber misalignment.

The variations in the torsion angle directly affect the effectiveness of stress transfer, with the fiber-matrix interface being a determining factor. The decrease in strength and modulus at an angle of 60° can be explained by the reduced contribution of fiber orientation and the reduction of effective fiber length (effective fiber length) according to the Kelly–Tyson theory. Meanwhile, the relatively stable change in modulus at 0° to 40° of twist angle consistent with the Halpin–Tsai prediction, which suggests that stiffness is strongly

influenced by the volume fraction and orientation of fibers.

The difference in tensile modulus between the two types of polymers is relatively small, so that the predicted Halpin-Tsai model value is obtained for short fiber (CSM) E_c = 3.0 GPa and longitudinal fiber (WR) E_c = 7.5 GPa. The actual fiber volume fraction (V_f) of the GFRP composite with a WR/CSM/WR/CSM configuration was 44%. These results show consistency between micromechanical theory and the structural characteristics of laminates, which confirms that the Halpin-Tsai model can be used as a reliable approach to predict the increase in stiffness due to fiber addition in glass fiber-reinforced composites in tensile testing.

The modulus of elasticity the GFRP composite in Figure 6(b) indicates that variations in the twist angle significantly influence its stiffness response. In both matrix systems, epoxy and polyester, there is a tendency for stiffness to increase at low angles, followed by a decrease at higher angles. This pattern indicates that fibers orientation remains effective in resisting flexural loads at minor angle (20°) deviations; however, its effectiveness decreases as the twist angle increases due to fibers misalignment and increasingly dominant stress redistribution. In general, the epoxy-based composite exhibits higher stiffness than the polyester, reflecting a better interfacial bond between the matrix and the fibers. This finding aligns with the principles of composite micromechanics, where changes in fibers orientation directly affect the load transfer capacity and effective modulus of the laminate.

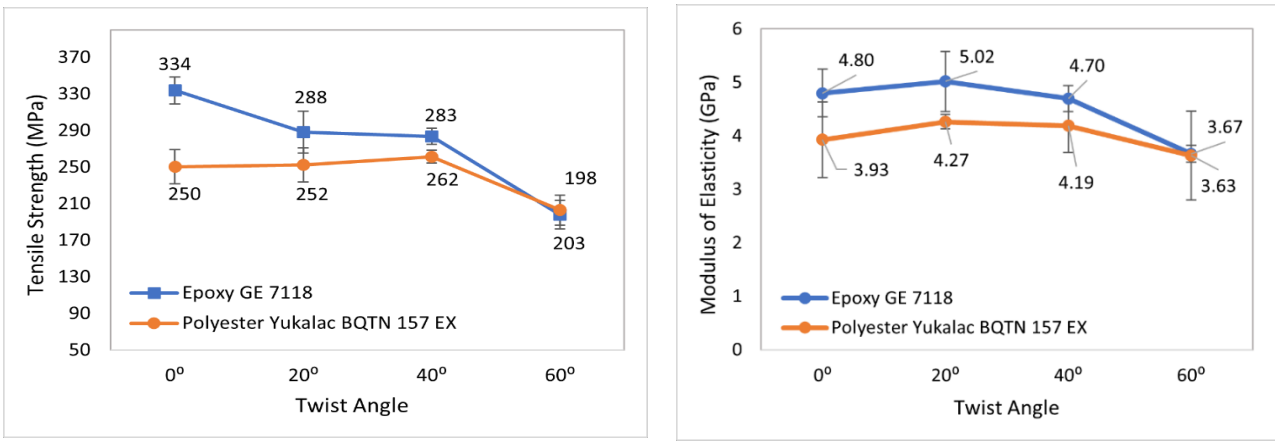

(a) (b)

Figure 6. Twist-tensile test of GFRP composite (n_WR = 2 and n_CSM = 2): (a) tensile strength and (b) modulus of elasticity

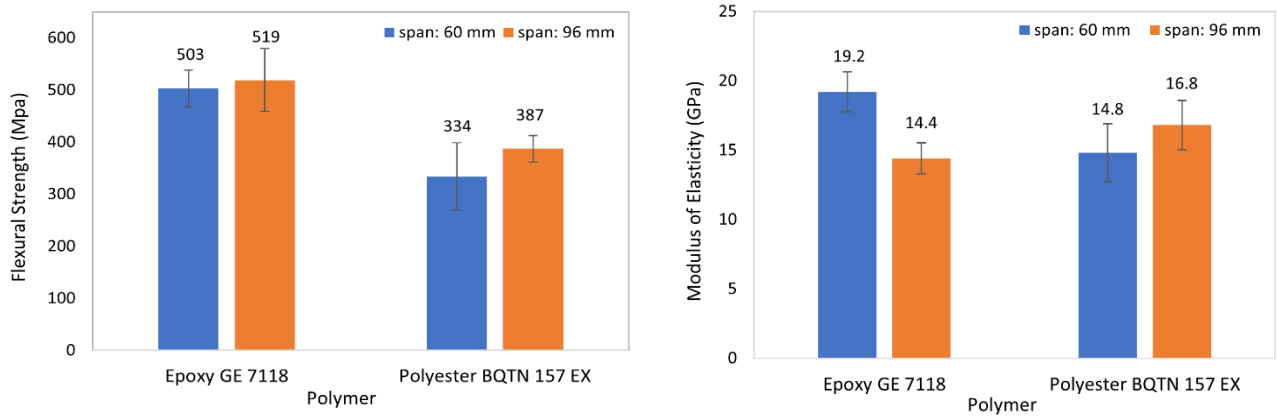

(a) (b)

Figure 7. Three-point bending behavior of the GFRP composite (n_WR = 5 and n_CSM = 5): (a) Flexural strength and (b) modulus of elasticity

These results are consistent with the study by Beter et al. [25], indicating that fiber orientation causes the fiber contribution to the tensile load to be distributed on the surface of the laminate composite. When the specimen was twisted at an angle below 45°, the resulting tensile response of the laminate composite was relatively more homogeneous due to the contributing fibers, which is a critical factor in determining the performance of the composite.

3.3 Flexural test analysis

The flexural test results for the two span configurations (96 mm and 60 mm) are displayed in Figure 7, demonstrating the consistent superiority of GFRP-epoxy composite (n_WR = 5 and n_CSM = 5) in flexural strength resistance, reaching 503 MPa at the short span and 519 MPa at the long span. It was compared to GFRP-polyester at 334 and MPa 387 MPa, respectively. However, the modulus of elasticity depicted different behavior. The results of the durability test show that the modulus of elasticity on epoxy are 14.4 GPa (long span) and 19.2 GPa (short span), while polyester is 14.8 GPa (short span) and 16.8 GPa (long span). This indicates that the flexural loading condition is highly susceptible to the span length, where shorter spans reduce the influence of rotation and

twisting shear, resulting in higher modulus values.

This difference was related to the contribution of shear deformation and the bending moment of the laminated composite. The shear resistance of GFRP-epoxy was superior to that of polyester, making it more resistant to bending loads and capable of larger deflection before failure. In contrast, GFRP-polyester exhibited higher stiffness but lower resilience, corresponding to its higher modulus of elasticity. Therefore, GFRP-epoxy is more suitable for applications requiring high flexural strength and good deflection capacity, while GFRP-polyester is preferable where structural stiffness is the primary concern.

The Halpin-Tsai predictions, it is observed that the model theoretically yields a modulus of approximately 7.0 G.Pa for the dominant fiber orientation ($\xi = 2$) and approximately 3.0 GPa for the random CSM orientation ($\xi = 2.L/d$). The significantly higher experimental values, indicate that the flexural response is not only controlled by the fiber–matrix micromechanics, but also by the structural contribution of the laminate, especially the WR layer which is dominant at the surface of the cross-section and increases the flexural stiffness. Thus, the difference between the theoretical predictions and the experimental results can be explained by a more complex flexural mechanism than the tensile one.

The span length in the three-point test significantly affected the composite material's flexural strength and modulus of elasticity. The results disclosed that at small span-to-thickness ratios (L/h), failure tended to be influenced by local deformation and compression, resulting in higher but less representative apparent strength values. However, at excessively large (L/h), local flexural failure predominated, deflection increased, and the measured strength and modulus of elasticity were likely to decline [26].

The difference in flexural modulus at various span lengths can be explained by the loading mechanism changing from fiber-dominated to matrix-dominated. At short spans, the bending response of GFRP-epoxy is primarily influenced by the outer fiber layer, exhibiting higher stiffness due to more efficient adhesion and load transfer. Conversely, at long spans, the components vibrate more, and the matrix plays a greater role in resisting the load. Polyester has a relatively larger shear modulus value at low–medium strains, so that GFRP-polyester composites can appear stiffer in long-span tests. It explains the phenomenon of span-dependent flexural behaviour seen in the experimental data.

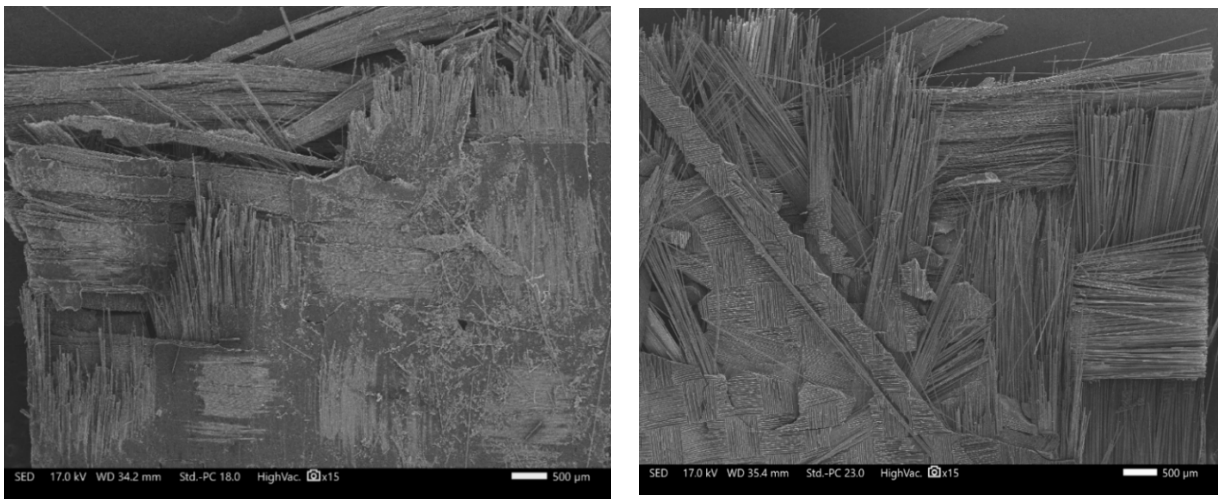

(a) (b)

Figure 8. SEM image after tensile test; (a) GFRP-epoxy failure mode (b) GFRP-polyester failure mode

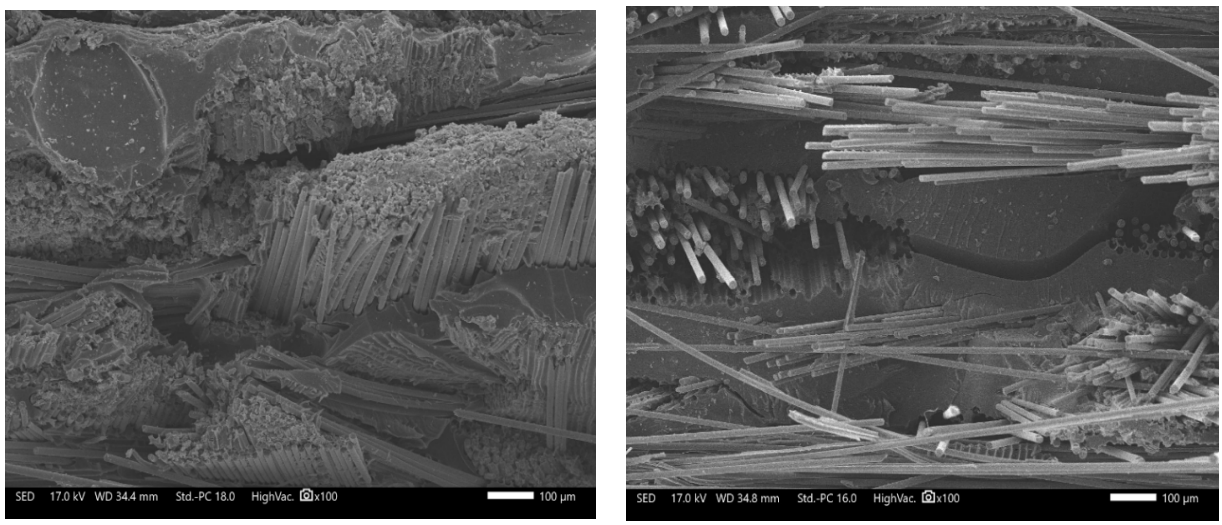

(a) (b)

Figure 9. SEM image after bending test; (a) GFRP-epoxy failure mode (b) GFRP-polyester failure mode

3.4 Failure modes microstructure analysis

The SEM images in Figure 8(a) shows the fracture morphology of the GFRP-epoxy composite (n_WR = 5 and n_CSM = 5) after a tensile test. It was afforded to fill the inter-fiber spaces, resulting in a strong matrix-fiber bond. In addition, some fibers fractured brittlely, while others exhibited fiber pull-out, indicating a combination of fiber damage and debonding mechanisms. The presence of fibers still encased in epoxy confirms the epoxy resin's good wetting ability than glass fibers.

Figure 8(b) demonstrates the failure modes of GFRP-polyester, showcasing significant damage of delamination, fiber pull-out, and split cracks in the matrix interface. These phenomena indicate a weak bond between the polyester resin and the glass fiber, generating suboptimal load transfer. Consequently, the material exhibited easier delamination fracture behavior. The polyester resin did not provide a good load distribution on the shear stress phenomena.

Figure 9(a) depicts the SEM fracture image after the flexural test. In the GFRP-epoxy composite, the matrix exhibited fiber-matrix interfacial bonding, characterized by effective wetting. The load tension distributed evenly from the matrix to the fiber was due to the load tension. Debonding was minimal and localized, in contrast to the GFRP-polyester, which disclosed more frequent debonding and fiber pull-out phenomena. In addition, brittle fiber fracture and homogeneous matrix damage confirm the structural compactness of the Epoxy. Overall, GFRP-epoxy could provide stronger bonds, more effective load distribution, and higher buckling resistance than polyester.

Figure 9(b) illustrates that the failure mode on the SEM image is dominant fiber pull-out, delamination, and debonding, indicating suboptimal interfacial bonding between the glass fibers and the polyester matrix, due to non-homogeneous resin wetting. This prevented efficient load transfer to the fibers but released through a pull-out mechanism. Debonding the fibers and leaving the imprint on the matrix indicates poor bonding. Its failure is highly dependent on the wetting ability of the polymer resin and fiber arrangements, which have a significant role in the failure behaviour [27-29].

According the Chowdhury et al. [30] and Matykiewicz et al. [31], during the curing process, epoxy resin forms a dense three-dimensional network through cross-linking. This structure produces polar groups, such as -OH (hydroxyl) and ether bonds (C-O-C) that interact strongly, including hydrogen bonds with silanol groups (Si-O-H) on the glass fiber surface. This combination strengthens interfacial adhesion and enhances the resin's load transfer ability, as evidenced by the minimal fiber pull-out phenomenon in SEM images.

In contrast, polyester resins use free radical polymerization, resulting in a sparser cross-linked network and fewer polar groups. It makes the interaction with the glass fibers primarily dependent on weaker van der Waals forces, resulting in a greater tendency for debonding and fibers pull-out in polyester-based composites.

3.5 Thermal stability of GFRP composite

The results of Thermogravimetric Analysis (TGA) and Derivative Thermogravimetry (DTG) tests on GFRP-polyester and GFRP-epoxy (Figures 10 and 11). The TGA chart shows differences in thermal resistance. Based on the TGA curve, GFRP-epoxy experiences degradation T_{onset} at temperatures around 340°C and T_{max} at range of 360–370°C, while GFRP-polyester begins to degrade at lower temperatures, around T_{onset} at 300°C and T_{max} at range of 350–360°C. It indicates that epoxy resin has higher thermal stability than polyester. The residual value of both, indicating a slower decomposition rate and better char formation. The DTG chart shows that GFRP-epoxy reaches a maximum decomposition rate (-0.6%/min) higher than GFRP-polyester (-0.4%/min). Although epoxy decomposes faster at peak temperatures, both composites exhibit good thermal resistance within the test temperature range. The sharper DTG peak in epoxy indicates a single-stage degradation process, while the wider peak in polyester indicates a slow and gradual decomposition process.

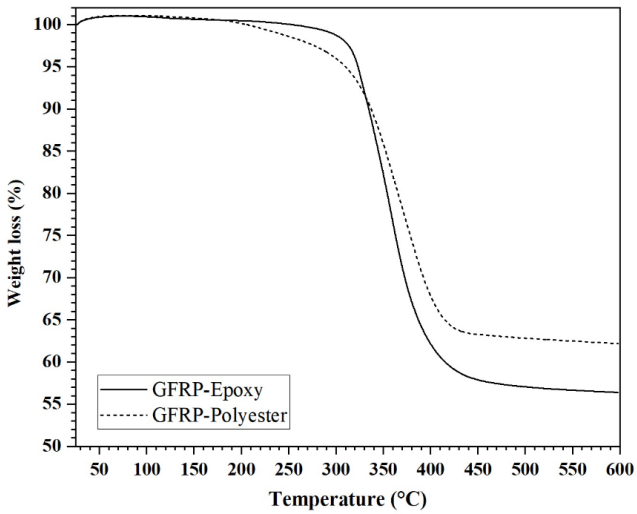

Figure 10. TGA chart determine weight loss, T_{onset} and $T_{maximum}$

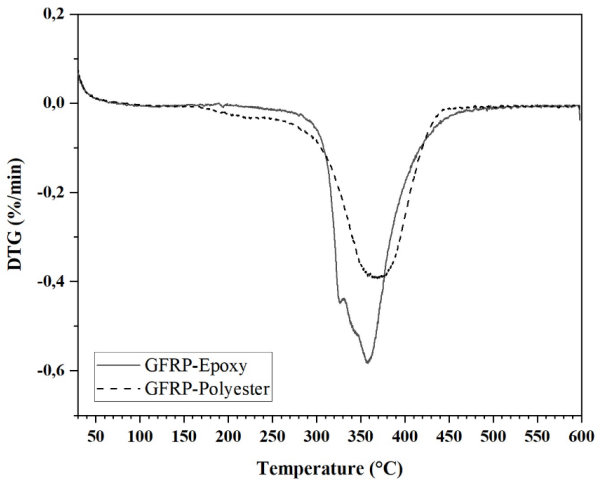

Figure 11. DTG chart determine maximum decomposition rate

Despite these characteristics, both materials have good thermal stability with the maximum temperature around 350°C, so they can be considered suitable for structural applications. These results are similar to the research of Yudhanto et al. [32] investigating thermal stability on glass fiber reinforced polyester, which obtained results of the initial temperature (T_{onset}) degradation of 300°C and the maximum temperature (T_{max}) degradation of 350°C. Then another

researcher, Boopalan et al. [33] reported that epoxy composites showed higher degradation temperatures and residual yields than polyester due to the denser cross-linked structure of epoxy.

The study of Braga and Magalhaes Jr [17] also supports the idea that adding glass fiber increases the thermal stability of both of resins. However, epoxy still showed better heat resistance to the matrix volatilisation process which initial degradation.

4. CONCLUSION

This study proves that the type of matrix resin significantly affects the mechanical performance of glass fiber laminated composites. The results show that GFRP-epoxy has higher tensile and flexural strengths than GFRP-polyester. In tensile-torsion tests, GFRP-epoxy achieved a maximum strength of 334 MPa, while GFRP-polyester was lower due to weak interfacial bonding. Flexural testing with various support spans showed that GFRP-epoxy had the best performance, with a maximum strength reaching 519 MPa. The results of SEM photo analysis of GFRP-epoxy showed a good fiber bond with the matrix and a more even load distribution. The GFRP-polyester showed a tendency for fiber pull-out and delamination. In terms of thermal resistance, GFRP-epoxy has a higher initial degradation temperature (340°C) than GFRP-polyester, indicating the material's ability to have good thermal resistance. GFRP-epoxy is superior for structural applications such as wind turbine blades, while GFRP-polyester is more suitable for non-structural components. The future work to investigate the effect environmental aging on the fatigue and bending-twist behavior on the interface of laminate sandwich composite.

ACKNOWLEDGMENT

The authors would like to express their gratitude to the Ministry of Higher Education, Science, and Technology, Republic of Indonesia (KEMDIKTISAINTEK), for providing funding support through the Fundamental Research Grant with Contract Number: 0498.07/LL5-INT/AL.04/2025. This support is highly significant in the implementation and completion of this research.

REFERENCES

[1] Kementerian Energi dan Sumber Daya Mineral Republik Indonesia. (2021). Keputusan Menteri Energi dan Sumber Daya Mineral Nomor 188.K/HK.02/MEM.L/2021 tentang Pengesahan Rencana Usaha Penyediaan Tenaga Listrik PT Perusahaan Listrik Negara (Persero) Tahun 2021 Sampai Dengan Tahun 2030 (RUPTL). Kementerian Energi dan Sumber Daya Mineral, Jakarta, 2021. https://jdih.esdm.go.id/dokumen/view?id=2192.

[2] Mishnaevsky Jr, L. (2022). Root causes and mechanisms of failure of wind turbine blades: Overview. Materials, 15(9): 2959. https://doi.org/10.3390/ma15092959

[3] Costa, A.M., Orosa, J.A., Vergara, D., Fernandez-Arias, P. (2021). New tendencies in wind energy operation and maintenance. Applied Sciences, 11(4): 1386. https://doi.org/10.3390/app11041386

[4] Cavalcanti, D.K., Banea, M.D., Neto, J.D.S.S., Lima, R.A.A. (2021). Comparative analysis of the mechanical and thermal properties of polyester and epoxy natural fibre-reinforced hybrid composites. Journal of Composite Materials, 55(12): 1683-1692. https://doi.org/10.1177/0021998320976811

[5] Zhao, Q., Yuan, Y., Sun, W., Fan, X., Fan, P., Ma, Z. (2020). Reliability analysis of wind turbine blades based on non-Gaussian wind load impact competition failure model. Measurement, 164: 107950. https://doi.org/10.1016/j.measurement.2020.107950

[6] Wang, W., Xue, Y., He, C., Zhao, Y. (2022). Review of the typical damage and damage-detection methods of large wind turbine blades. Energies, 15(15): 5672. https://doi.org/10.3390/en15155672

[7] Chung, P.D. (2021). Smoothing the power output of a wind turbine group with a compensation strategy of power variation. Engineering, Technology & Applied Science Research, 11(4): 7343-7348. https://doi.org/10.48084/etasr.4234

[8] Laux, T., Cappello, R., Callaghan, J., Olafsson, G., et al. (2023). Testing of a wind turbine blade spar cap to web joint subcomponent subjected to multiaxial loading. https://eprints.soton.ac.uk/481968/1/ICCM23_Full_Paper_Laux_final.pdf.

[9] Morăraș, C.I., Goanță, V., Istrate, B., Munteanu, C., Dobrescu, G.S. (2022). Structural testing by torsion of scalable wind turbine blades. Polymers, 14(19): 3937. https://doi.org/10.3390/polym14193937

[10] Chen, X., Zhao, W., Zhao, X.L., Xu, J.Z. (2014). Failure test and finite element simulation of a large wind turbine composite blade under static loading. Energies, 7(4): 2274-2297. https://doi.org/10.3390/en7042274

[11] Morăraș, C.I., Goanță, V., Husaru, D., Istrate, B., Bârsănescu, P.D., Munteanu, C. (2023). Analysis of the effect of fiber orientation on mechanical and elastic characteristics at axial stresses of GFRP used in wind turbine blades. Polymers, 15(4): 861. https://doi.org/10.3390/polym15040861

[12] Olabi, A.G., Wilberforce, T., Elsaid, K., Sayed, E.T., Salameh, T., Abdelkareem, M.A., Baroutaji, A. (2021). A review on failure modes of wind turbine components. Energies, 14(17): 5241. https://doi.org/10.3390/en14175241

[13] Couto, L.D.L., Moreira, N.E., Saito, J.Y.D.O., Hallak, P.H., Lemonge, A.C.D.C. (2023). Multi-objective structural optimization of a composite wind turbine blade considering natural frequencies of vibration and global stability. Energies, 16(8): 3363. https://doi.org/10.3390/en16083363

[14] Grammatikos, S.A., Jones, R.G., Evernden, M., Correia, J.R. (2016). Thermal cycling effects on the durability of a pultruded GFRP material for off-shore civil engineering structures. Composite Structures, 153: 297-310. https://doi.org/10.1016/j.compstruct.2016.05.085

[15] Stanciu, M.D., Nastac, S.M., Tesula, I. (2022). Prediction of the damage effect on fiberglass-reinforced polymer matrix composites for wind turbine blades. Polymers, 14(7): 1471. https://doi.org/10.3390/polym14071471

[16] Chen, X., Berring, P., Madsen, S.H., Branner, K., Semenov, S. (2019). Understanding progressive failure mechanisms of a wind turbine blade trailing edge section through subcomponent tests and nonlinear FE analysis.

Composite Structures, 214: 422-438. https://doi.org/10.1016/j.compstruct.2019.02.024
[17] Braga, R.A., Magalhaes Jr, P.A.A. (2015). Analysis of the mechanical and thermal properties of jute and glass fiber as reinforcement epoxy hybrid composites. Materials Science and Engineering: C, 56: 269-273. https://doi.org/10.1016/j.msec.2015.06.031
[18] Chichane, A., Boujmal, R., El Barkany, A. (2023). A comparative study of analytical and numerical models of mechanical properties of composites and hybrid composites reinforced with natural reinforcements. Polymers and Polymer Composites, 31: 09673911231172491. https://doi.org/10.1177/09673911231172491
[19] Abdurohman, K., Pratomo, R.A., Hidayat, R., Ramadhan, R.A., Nurtiasto, T.S., Ardiansyah, R., PPP, M.G. (2023). A comparison of vacuum infusion, vacuum bagging, and hand lay-up process on the compressive and shear properties of GFRP materials. Indonesian Journal of Aerospace, 21(1): 39-50. https://doi.org/10.59981/ijoa.2023.286
[20] Yudhanto, F. (2021). Effect of addition microcrystalline cellulose on mechanical properties of jute/glass fibers hybrid laminated composite. International Journal of Automotive Engineering, 12(1): 1-8. https://doi.org/10.20485/jsaeijae.12.1_1
[21] Ma, Z., Zhang, P., Zhu, J. (2022). Comparative studies on the effect of fabric structure on mechanical properties of carbon fiber/epoxy composites. Journal of Industrial Textiles, 51(1_suppl): 1348S-1371S. https://doi.org/10.1177/1528083720987517
[22] Ma, Z., Man, R., Yin, D., Cheng, L., Ma, W., Jia, C. (2023). Effect of curing process on tensile and flexural properties of 3D woven structural polymer composites. Fibers and Polymers, 24(8): 2835-2848. https://doi.org/10.1007/s12221-023-00259-9
[23] Laureto, J.J., Pearce, J.M. (2018). Anisotropic mechanical property variance between ASTM D638-14 type i and type iv fused filament fabricated specimens. Polymer Testing, 68: 294-301. https://doi.org/10.1016/j.polymertesting.2018.04.029
[24] ASTM, I. (2007). Standard test methods for flexural properties of unreinforced and reinforced plastics and electrical insulating materials. ASTM D790-07.
[25] Beter, J., Schrittesser, B., Meier, G., Lechner, B., Mansouri, M., Fuchs, P.F., Pinter, G. (2020). The tension-twist coupling mechanism in flexible composites: A systematic study based on tailored laminate structures using a novel test device. Polymers, 12(12): 2780. https://doi.org/10.3390/polym12122780
[26] Liu, C., Du, D., Li, H., Hu, Y., et al. (2016). Interlaminar failure behavior of GLARE laminates under short-beam three-point-bending load. Composites Part B: Engineering, 97: 361-367. https://doi.org/10.1016/j.compositesb.2016.05.003
[27] Arabi, N. (2018). Static and cyclic performance of cementitious composites reinforced with glass-fibres. Materiales de construccion, 68(329): 146-146. https://doi.org/10.3989/mc.2018.10216
[28] Palizvan, M., Tahaye Abadi, M., Sadr, M.H. (2020). Micromechanical damage behavior of fiber-reinforced composites under transverse loading including fiber-matrix debonding and matrix cracks. International Journal of Fracture, 226(2): 145-160. https://doi.org/10.1007/s10704-020-00484-w
[29] Talreja, R. (2024). Failure Analysis of Composite Materials with Manufacturing Defects. CRC Press. https://doi.org/10.1201/9781003225737
[30] Chowdhury, S.C., Prosser, R., Sirk, T.W., Elder, R.M., Gillespie Jr, J.W. (2021). Glass fiber-epoxy interactions in the presence of silane: A molecular dynamics study. Applied Surface Science, 542: 148738. https://doi.org/10.1016/j.apsusc.2020.148738
[31] Matykiewicz, D., Dudziec, B., Skórczewska, K., Sałasińska, K. (2024). The effect of silanes treatments on thermal and mechanical properties of nettle fibre/bio epoxy composites. Journal of Natural Fibers, 21(1): 2332913. https://doi.org/10.1080/15440478.2024.2332913
[32] Yudhanto, F., Yudha, V., Budiyantoro, C., Jamasri, J., Priyahapsara, I., Ogah, A., Ridzuan, M.J.M. (2024) Effect of stacking sequence on the hybrid laminated composite for savonius wind turbine blades. International Review of Mechanical Engineering, 18(12): 615-624. https://doi.org/10.15866/ireme.v18i12.24531
[33] Boopalan, M., Niranjanaa, M., Umapathy, M.J. (2013). Study on the mechanical properties and thermal properties of jute and banana fiber reinforced epoxy hybrid composites. Composites Part B: Engineering, 51: 54-57. https://doi.org/10.1016/j.compositesb.2013.02.033

NOMENCLATURE

%/min.	Weight loss rate
L/d	Aspect Ratio
V_f	Fiber volume fraction (%)
wt.%	Weight percentage
E	Modulus (GPa)

Subscripts

T_{onset}	Initial degradation
T_{max}	Maximum degradation
*n*_CSM	Number of layers of Chopped Strand Mat
*n*_WR	Number of layers of Woven Roving
ή	Reinforcement factor
ξ	Shape orientation parameter